Forecast Skill of the South American Monsoon System

CHARLES JONES

Earth Research Institute, University of California, Santa Barbara, Santa Barbara, California

LEILA M. V. CARVALHO

Earth Research Institute, and Department of Geography, University of California, Santa Barbara, Santa Barbara, California

BRANT LIEBMANN

Cooperative Institute for Research in Environmental Sciences Climate Diagnostics Center, Boulder, Colorado

(Manuscript received 1 October 2011, in final form 1 December 2011)

ABSTRACT

The South American monsoon system (SAMS) is the most important climatic feature in South America and is characterized by pronounced seasonality in precipitation. This study uses the National Centers for Environmental Prediction Climate Forecast System, reforecasts version 2 (CFSRv2), to investigate the skill of probabilistic forecasts of onset and demise dates, duration, and amplitude of SAMS during 1982–2009. A simple index based on the empirical orthogonal function of precipitation anomalies is employed to characterize onsets, demises, durations, and amplitudes of SAMS. The CFSv2 model has useful skill to forecast seasonal changes in SAMS. Probabilistic forecasts of onset and demise dates have 16.5% and 43.3% improvements, respectively, over climatological forecasts. Verification of hindcasts of durations and amplitudes of SAMS shows relatively small biases and root-mean-square errors.

1. Introduction

The monsoon in South America [hereafter the South American monsoon system (SAMS)] has an important role for the millions of people leaving in the continent (Carvalho et al. 2002, 2011a; Vera et al. 2006b). The seasonal precipitation in SAMS is critical for agriculture, hydroelectric power generation, and water resources in urban regions (Mechoso et al. 2005; Marengo et al. 2010). The hydrological cycle over the Amazon basin and central Brazil involves an intricate set of processes. Drought conditions due to delayed onsets of SAMS and below-average precipitation during the monsoon can severely affect ecosystems (Zeng et al. 2008; Marengo et al. 2011). Furthermore, SAMS has experienced significant multiannual changes in recent decades (Grimm and Natori 2006; Marengo 2009; Carvalho et al. 2011c, unpublished manuscript, hereafter C11c; 2011b), thus motivating research to determine the roles of natural variability and anthropogenic forcing (Vera et al. 2006a; Silva et al. 2008; Bombardi and Carvalho 2009; Marengo et al. 2009).

The National Centers for Environmental Prediction (NCEP) upgraded the Climate Forecast System model to a new version (CFSv2; Saha et al. 2006, 2010; S. Saha et al. 2011, personal communication). CFSv2 brings many important changes in physical parameterizations and atmosphere–ocean data assimilation (S. Saha et al. 2011, personal communication). To further understand model performance and improve model calibration for seasonal forecasts, NCEP has produced reforecasts in the period 1982–2010 (S. Saha et al. 2011, personal communication). Yuan et al. (2011) determined that globally CFSv2 has better forecast skill for precipitation and temperature at 1-month lead (37% and 29%, respectively) than the previous CFS.

The objective of this study is to investigate the forecast skill of SAMS using CFS reforecasts. We focus on the large-scale characteristics of SAMS, and a simple

Corresponding author address: Dr. Charles Jones, Earth Research Institute, University of California, Santa Barbara, Santa Barbara, CA 93106.
E-mail: cjones@eri.ucsb.edu

DOI: 10.1175/JCLI-D-11-00586.1

© 2012 American Meteorological Society

index based on precipitation anomalies is used to characterize the onset and demise dates, duration, and amplitude of SAMS. Probabilistic forecasts are developed for the period 1982–2009 and are validated against observed onset and demise dates, duration, and amplitude. Section 2 describes the datasets. Section 3 discusses the methodology, forecasts, and validation procedures. Conclusions are presented in section 4.

2. Data

Forecasts of SAMS characteristics are verified with observed daily gridded precipitation from the Climate Prediction Center unified gauge (CPC-uni) dataset (January 1982–December 2010). The CPC-uni uses an optimal interpolation technique to reproject precipitation reports to a grid (Chen et al. 2008; Silva et al. 2011). The original grid spacing is 0.5° latitude–longitude and bilinear interpolation is used to downgrade the data to 1.0° latitude–longitude for consistency with the grid spacing of the NCEP CFS reforecasts (126 spectral triangular truncation ~0.937° latitude × longitude, 64 levels). It is important to note, however, that some differences exist among precipitation datasets over South America as discussed in Carvalho et al. (2012). Nevertheless, the annual cycle of SAMS (i.e., onset, demise, duration, and amplitude) obtained from CPC-uni is consistent with other datasets based on surface stations or satellite data (Carvalho et al. 2012).

The forecast skill of SAMS characteristics is investigated with reforecasts from the NCEP CFS model version 2 (CFSRv2). Since the main objective of this study is to evaluate the forecast skill of seasonal characteristics of SAMS (i.e., onset, duration, demise, and amplitude), 9-month hindcasts of precipitation initialized every fifth day (3rd, 8th, 13th, 18th, 23rd, and 28th) and four cycles (0000, 0600, 1200, and 1800 UTC) per day during September 1982–2009 are analyzed (1344 forecasts of 9-month lead times each). The 9-month hindcasts with initial conditions in September capture the entire monsoon season and therefore are suitable to evaluate the forecast skill of the features described above. These forecasts are additionally reduced by computing mean daily precipitation as the average of four samples per day (0000, 0600, 1200, and 1800 UTC).

3. Results

The forecast skill of SAMS is examined by focusing on the following large-scale features: dates of onset and demise, duration, and amplitude of the monsoon. These characteristics are determined with an empirical orthogonal function (EOF) analysis of daily CPC-uni precipitation (Wilks 2006). Before computation of EOF analysis, time series of precipitation in each grid point are scaled by the square root of the cosine of the latitude and the long-term (1982–2010) mean removed. EOF is then computed only with precipitation anomalies from land grid points.

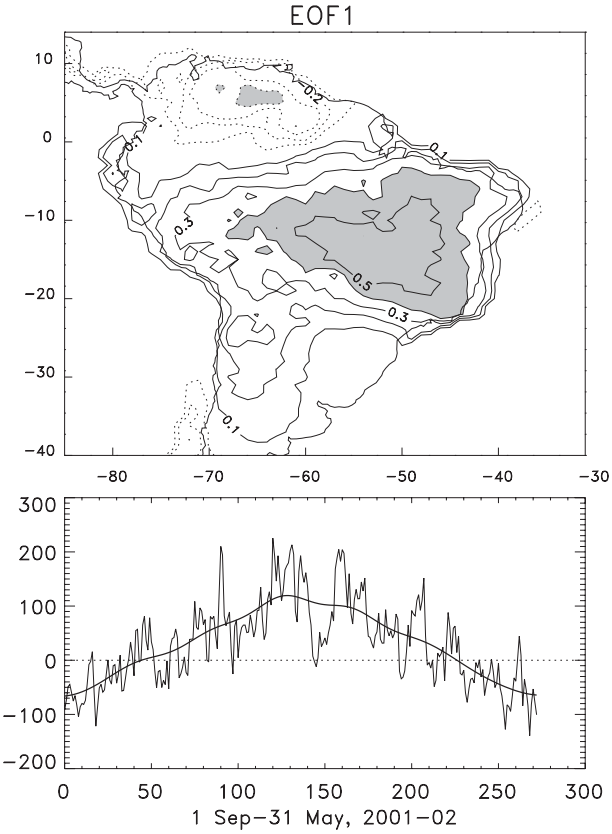

FIG. 1. (top) First EOF patterns described as correlations between the first time coefficients (PC1) and precipitation anomalies. Solid (dashed) contours indicate positive (negative) correlations at 0.1 intervals (zero contours omitted). Shadings indicate correlations greater (less) than 0.4 (−0.4). (bottom) An example of PC1 (thin solid; dimensionless). The thick solid line indicates smoothed PC1 (10 passes of a 15-day moving average). Period: daily, January 1982–December 2010.

The first mode (EOF1) captures 8.8% of the total precipitation variance (Fig. 1, top). The EOF1 spatial pattern is characterized by large positive loadings over central eastern Brazil and negative values over the northern parts of South America. EOF1 is statistically separated from the second mode (not shown), which is associated with the variability of precipitation over southeastern Brazil especially in the South Atlantic convergence zone (SACZ). Note that the EOF domain in Fig. 1 is not the same as the one studied by Carvalho et al. (2011a; C11c; Carvalho et al. 2012) and Silva and Carvalho (2007); we note that the largest correlations between PC1 and

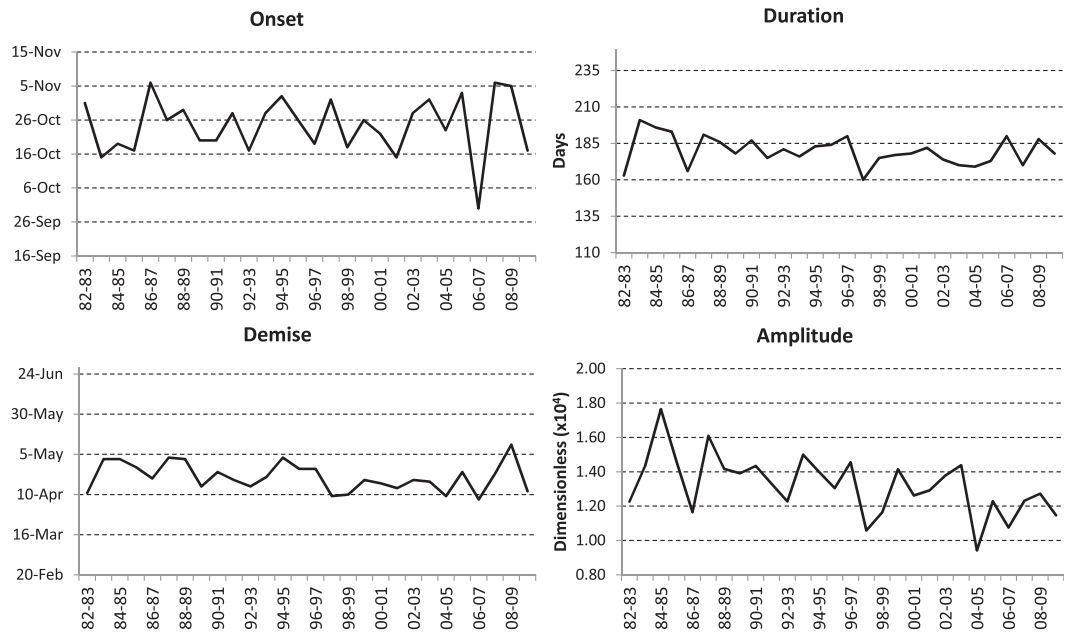

FIG. 2. The onset, duration (days), demise, and amplitude (dimensionless) of SAMS as determined by the first EOF of precipitation.

precipitation (Fig. 1) is slightly displaced eastward with respect to the domain used in those studies. Carvalho et al. (2012). showed that there is a positive trend in vertically integrated moisture divergence east of the Amazon (1979–2010) with high correlations with the first EOF calculated in that study, which suggests that the onset, amplitude, and duration of the monsoon over eastern Amazon are influenced by the weakening of the trade winds and increase in vertically integrated moisture divergence.

The large-scale features of onset, demise, duration, and amplitude are derived from the first principal component (PC1). To illustrate the procedure, Fig. 1 (bottom) shows a segment of PC1 for the period 1 September–31 May 2001/02. Also indicated, is a smoothed PC1 obtained with 10 passes of a 15-day moving average. This smoothing procedure is obtained empirically and used to decrease the influence of high-frequency variations during the transition phases of SAMS. The large-scale onset of SAMS is defined here as the date when the smoothed PC1 changes from negative to positive values. This implies that positive precipitation anomalies during that time become dominant over the SAMS domain. Likewise, the demise of SAMS is defined as the date when the smoothed PC1 changes from positive to negative values. The duration of the monsoon is defined as the period between onset and demise dates. Last, the amplitude of the monsoon is defined as the integral of positive unsmoothed PC1 values from onset to demise. Therefore, the amplitude index represents the sum of positive precipitation anomalies and minimizes the effect of "break" periods in the monsoon especially near the onset and demise. Break periods are particularly frequent on intraseasonal time scales (Jones and Carvalho 2002).

Figure 2 shows the observed onset and demise dates, duration, and amplitude. The median onset in 1982–2009 was in late October and varied from 1 October (2006/07) to 7 November (1986/87, 2007/08). The median demise date is in late April and varied from early April to early May in 1982–2009. Accordingly, the duration of SAMS varies as follows: median of 178 days, minimum of 160 days, and maximum of 201 days. The median amplitude (dimensionless) is 1.32, the minimum is 0.94, and the maximum is 1.76. While Fig. 2 indicates a negative trend in amplitude, there are significant regional differences in trends over the SAMS domain as discussed in detail by C11c.

Forecasts of onset, demise, duration, and amplitude are derived from the NCEP CFS hindcasts using the following approach:

- Each forecast of daily average precipitation is projected onto the observed EOF1 (Fig. 1, top) resulting in a forecast of PC1 ($PC1_{FCS}$) (time series are 9 months in length). For each summer season, there are 24 members initialized in September (6 initial conditions every fifth day × four cycles).
- The mean forecast bias is computed as

$$\mathrm{BIAS}(t) = 1/N \sum_{i=1}^{N} [\mathrm{PC1}_{\mathrm{OBS}}(t) - \mathrm{PC1}^{i}_{\mathrm{FCS}}(t)],$$

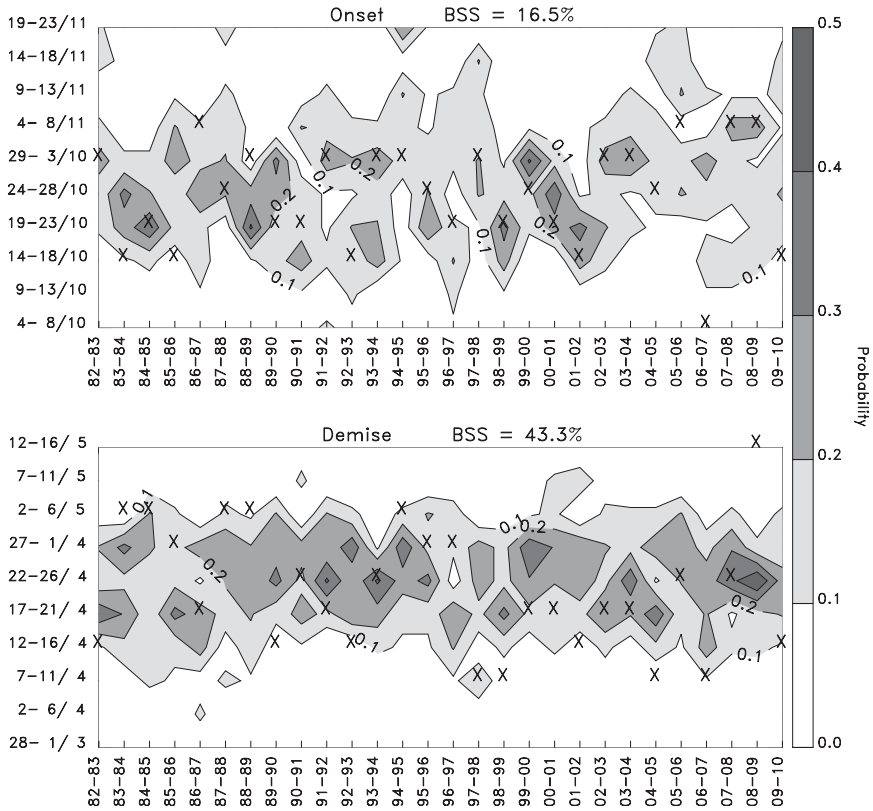

FIG. 3. (top) Shading indicates probabilistic forecasts of SAMS onset. The vertical axis is the onset date in a 5-day window and the horizontal axis shows seasons (1982–2010). Observed dates of onset are indicated by "×." (bottom) As in (top), but for probabilistic forecasts of the SAMS demise. BSS are indicated at the top of each and represent improvements upon forecasts using climatology.

where $PC1_{OBS}$ = observed PC1, i = forecast member, t = lead time from 1 to ~270 days, and N = 1344 members. To minimize the effect of noise, the mean bias is further smoothed with 300 passes of a 1–2–1 moving average. Next, the mean bias (not shown) is removed from each 9-month forecast of PC1.

Each bias-corrected $PC1_{FCS}$ is smoothed with 10 passes of a 15-day moving average and forecasts of the onset, demise, duration, and amplitude are determined as explained above. Since the forecasts for the onset and demise are both produced about a month before the onset, the lead time for the onset forecast is much shorter than the lead time for the demise forecast (~1 month versus ~1 month + the median duration of ~178 days).

Since the definitions of onset and demise dates previously discussed involve arbitrary criteria, it is not realistic and useful to forecast exact dates of onsets and demises of SAMS. In contrast, probabilistic forecasts of the onset and demise are performed for predefined time intervals. The following onset windows are defined: 4–8, 9–13, 14–18, 19–23, 24–28 October; 29 October–3 November; 4–8, 9–13, 14–18, and 19–23 November. From the observational record (Fig. 2), the median onset window is on 24–28 October and the climatological probability of onset on that window is $\Gamma_{ONSET} = 0.11$ (i.e., the number of onsets on this window divided by the number of onsets). Likewise, the following demise windows are defined: 28 March–1 April; 2–6, 7–11, 12–16, 17–21, 22–26 April; 27 April–1 May; 2–6, 7–11, and 12–16 May. The median demise date is on 17–21 April and the climatological probability of demise on that window is $\Gamma_{DEMISE} = 0.21$.

Probabilistic forecasts of onset are computed as $y_i = O_i/\mathrm{Mb}$, where O_i is the number of members forecasting onset in window i and Mb = 24 the total number of members during each September; likewise for forecasts of the demise of SAMS.

The probabilistic forecasts of the onset were validated with the Brier skill score (BSS; Wilks 2006) defined as

$$\mathrm{BSS} = 1 - \frac{\mathrm{BS}}{\mathrm{BS}_{\mathrm{Ref}}}, \quad \mathrm{BS} = \frac{1}{T}\sum_{k=1}^{T}(y_k - O_k),$$

$$\mathrm{BS}_{\mathrm{Ref}} = \Gamma_{\mathrm{ONSET}}(1 - \Gamma_{\mathrm{ONSET}}),$$

where BS is the Brier score, y_k is the forecast probability, O_k is the observation (1 = onset on window i, 0 = no onset in window i), $T = 280$ forecasts (10 windows × 28 seasons), BS_{Ref} is the reference Brier score, and Γ_{ONSET} is the climatological probability of onset; similarly for validation of probabilistic forecasts of demise of SAMS.

Figure 3 (top) shows probabilistic forecasts of the SAMS onset for each summer season during 1982–2010. Note that to simplify the procedure, if the probability of the onset is for earlier (later) than 4–8 October (19–23 November), the forecast is included in the first (last) time window. The observed onset of SAMS is indicated by "×." One notes that the ensemble members have moderate spread with forecast probabilities concentrating between [0.2–0.5]. Furthermore, the onset verification is typically contained within these values of probabilities. Interestingly, several hindcasts exhibit remarkable success in forecasting the onset of SAMS (e.g., 1984/85, 1991/92, 1993/94, 2002/03, 2003/04, 2007/08, and 2008/09). Nevertheless, some obvious problems are apparent such that the spread among the members is high and the forecasts completely miss the onset of SAMS (e.g., 1985/86, 1986/87, 1996/97, 2004/05, 2005/06, 2006/07, and 2009/10). The BSS of probabilistic forecasts of SAMS gives 16.5% improvement over climatological forecasts (i.e., a forecaster would always forecast the median onset on 24–28 October).

Probabilistic forecasts of SAMS demise as well as verification dates are shown in Fig. 3 (bottom). Comparatively, the spread among ensemble members of the SAMS demise is less than the spread of forecasts of the onsets as indicated by probabilities in the [0.1–0.2] interval. As in the previous case, some hindcasts are quite successful in forecasting the demise of SAMS (e.g., 1993/94, 1993/94, and 2007/08), while others are much less skillful (e.g., 1983/84, 1988/89, 2001/02, 2004/05, and 2008/09). Interestingly, BSS = 43.3% for probabilistic forecasts of the demise, which gives a much higher improvement over climatological forecasts.

The quality of the probabilistic forecasts is further assessed by computing attribute diagrams (Wilks 2006). Two calibration distributions are computed: observed frequency conditioned on the values of the forecasts and frequency of use of forecasts (or refinement distributions). The calculations are done separately for probabilistic forecasts of the onset and demise. Figure 4 (top) shows the calibration functions for hindcasts of the onset and indicates that the forecasts are relatively well calibrated with only moderate conditioned biases. Numbers in parentheses indicate the relative frequency of the use of forecasts (i.e., the frequency in which probabilistic forecasts in the bin range are issued). Deviations from the 1:1 line occur at forecast probabilities of 0.2 and are indicative of underforecasting (i.e., observations occur more frequently than forecasted). It is also noteworthy that because of the spread among the ensemble members, forecast probabilities greater than 0.42 are never issued. The calibration functions for hindcasts of the demise are shown in Fig. 4 (bottom) and indicate significant deviations

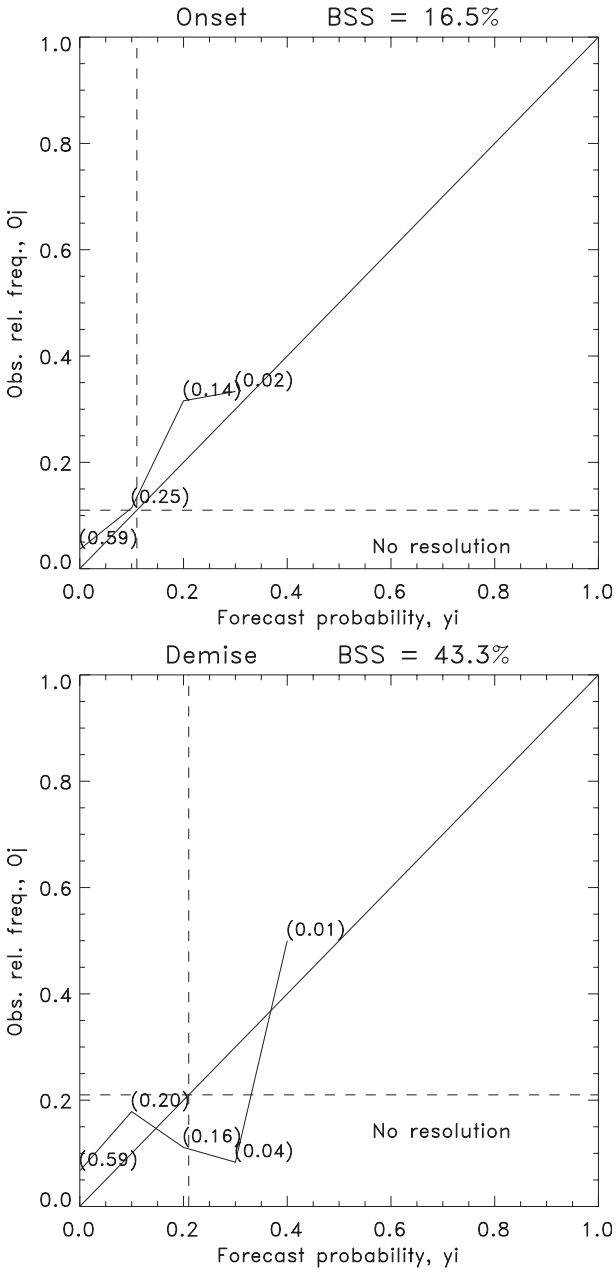

FIG. 4. Attribute diagrams of probabilistic forecasts of the SAMS (top) onset and (bottom) demise. Curves show observed relative frequency of SAMS onset (demise) conditional on six possible probability forecasts. Perfect reliability is indicated by 1:1 line. The numbers in parentheses show the relative frequency of the use of forecast values $p(y_i)$.

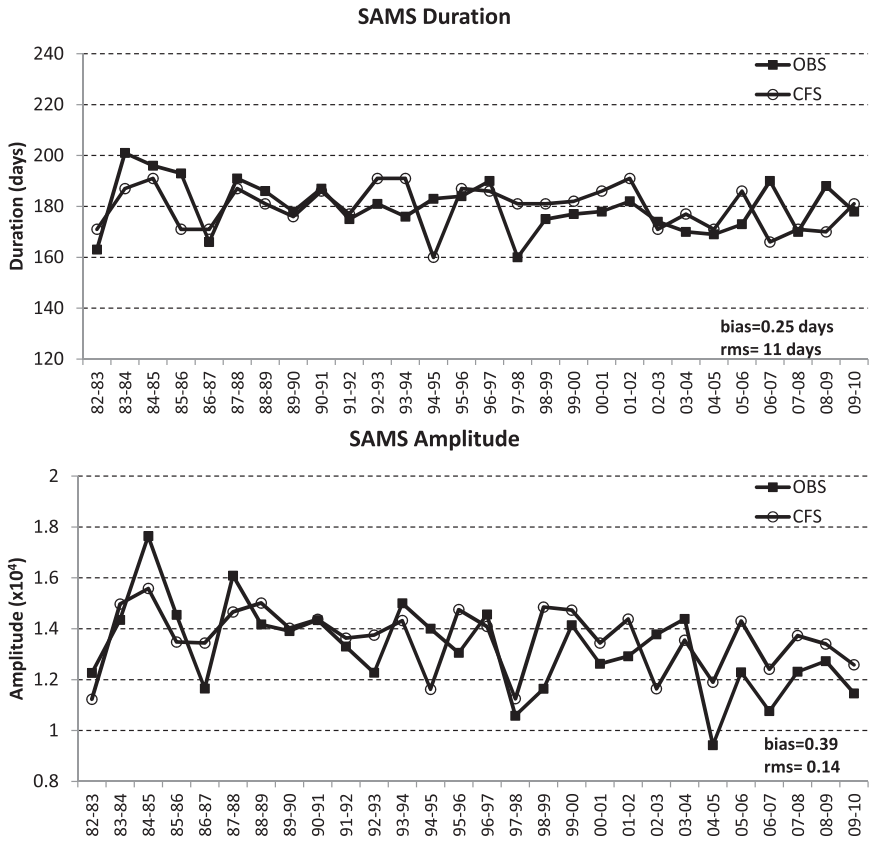

FIG. 5. Hindcasts of SAMS (top) duration and (bottom) amplitude for each summer season during 1982–2010. CFS forecasts (observations) are indicated by solid lines with open circles (solid with squares). Biases and root-mean-square errors (rms) are indicated on the insets of each.

from the 1:1 line for forecast probabilities between [0.2–0.3] exhibiting overforecasting characteristics. Similarly, forecast probabilities of the demise greater than 0.5 are never issued.

Hindcasts of SAMS duration D_K for each summer season are computed as

$$D_K = (\text{Demise}_j - \text{Onset}_i),$$

where Demise_j and Onset_i are the demise and onset time windows with the largest forecast probabilities. For example, suppose the forecasts of the demise windows for the 1984/85 season are: 0.000, 0.000, 0.0833, 0.125, 0.333, 0.167, 0.167, 0.125, 0.000, and 0.000. Then, the fifth demise window is selected (17–21 May), since there is more consensus among the ensemble members for that demise window. Likewise, suppose the forecast probabilities for the onset window for the 1984/85 season are 0.042, 0.0833, 0.0417, 0.167, 0.125, 0.250, 0.208, 0.0833, 0.000, and 0.000. Then, the sixth onset window is selected (29 October–3 November). The duration is then the interval between the onset and demise.

Likewise, hindcasts of amplitudes A_K are calculated as the average amplitude from the ensemble members that contribute to the largest forecast probabilities of Demise_j and Onset_i. Hindcasts and verifications of SAMS duration (Fig. 5, top) indicate skillful forecasts with a mean bias of 0.25 days and a root-mean square (rms) error of 11 days. Likewise, hindcasts and verifications of SAMS amplitudes (Fig. 5, bottom) show a mean bias of 0.39 and an rms error of 0.14. It is worth noting that probabilistic forecasts derived from the NCEP CFS reforecasts are particularly successful in capturing some interannual changes in SAMS (e.g., 1982/83 and 1997/98), since there is a significant change in the SAMS amplitude.

4. Summary and conclusions

This study uses CFSRv2 reforecasts to analyze the skill of probabilistic forecasts of large-scale characteristics of SAMS, namely the onset and demise dates, duration, and amplitude. A simple index is constructed to characterize these properties and is equally applied to forecasts and observations. The results indicate that the CFSv2 model

has useful skill to forecast seasonal changes in SAMS. Probabilistic forecasts of the onset and demise dates have 16.5% and 43.3% improvements, respectively, over climatological forecasts and relatively small biases and errors in durations and amplitudes. Seasonal forecasts of regional onsets and demises within SAMS are important, but have not been addressed here. Since EOF1/PC1 represent the large-scales aspects of SAMS, other indices can effectively characterize regional variations in the onsets and demises over the SAMS (e.g., Liebmann and Marengo 2001; Nieto-Ferreira and Rickenbach 2011). The authors are currently investigating these aspects and results will be reported in the future.

Acknowledgments. The authors thank the support of NOAA's Climate Program Office (Grants NA07OAR4310211 and NA10OAR4310170). The authors greatly acknowledge the support from NCEP, CPC, the Climate Test Bed, and NCDC for making the datasets available.

REFERENCES

Bombardi, R. J., and L. M. V. Carvalho, 2009: IPCC global coupled climate model simulations of the South America monsoon system. *Climate Dyn.,* **33,** 893–916.

Carvalho, L. M. V., C. Jones, and M. A. F. Silva Dias, 2002: Intraseasonal large-scale circulations and mesoscale convective activity in tropical South America during the TRMM-LBA campaign. *J. Geophys. Res.,* **107,** 8042, doi:10.1029/2001JD000745.

——, A. E. Silva, C. Jones, B. Liebmann, P. L. Silva Dias, and H. R. Rocha, 2011a: Moisture transport and intraseasonal variability in the South America monsoon system. *Climate Dyn.,* **36,** 1865–1880, doi:10.1007/s00382-00010-00806-00382.

——, C. Jones, A. E. Silva, B. Liebmann, and P. L. Silva Dias, 2011b: The South American monsoon system and the 1970s climate transition. *Int. J. Climatol.,* **31,** 1248–1256, doi:10.1002/joc.2147.

——, ——, A. N. Posadas, R. Quiroz, B. Bookhagen, and B. Liebmann, 2012: Precipitation characteristics of the South American monsoon system derived from multiple datasets. *J. Climate,* in press.

Chen, M. Y., W. Shi, P. P. Xie, V. B. S. Silva, V. E. Kousky, R. W. Higgins, and J. E. Janowiak, 2008: Assessing objective techniques for gauge-based analyses of global daily precipitation. *J. Geophys. Res.,* **113,** D04110, doi:10.1029/2007JD009132.

Grimm, A. M., and A. A. Natori, 2006: Climate change and interannual variability of precipitation in South America. *Geophys. Res. Lett.,* **33,** L19706, doi:10.1029/2006GL026821.

Jones, C., and L. M. V. Carvalho, 2002: Active and break phases in the South American monsoon system. *J. Climate,* **15,** 905–914.

Liebmann, B., and J. Marengo, 2001: Interannual variability of the rainy season and rainfall in the Brazilian Amazon basin. *J. Climate,* **14,** 4308–4318.

Marengo, J. A., 2009: Long-term trends and cycles in the hydrometeorology of the Amazon basin since the late 1920s. *Hydrol. Processes,* **23,** 3236–3244.

——, R. Jones, L. M. Alves, and M. C. Valverde, 2009: Future change of temperature and precipitation extremes in South America as derived from the PRECIS regional climate modeling system. *Int. J. Climatol.,* **29,** 2241–2255.

——, and Coauthors, 2010: Recent developments on the South American monsoon system. *Int. J. Climatol.,* **32,** 1–21, doi:10.1002/joc.2254.

——, J. Tomasella, L. M. Alves, W. R. Soares, and D. A. Rodriguez, 2011: The drought of 2010 in the context of historical droughts in the Amazon region. *Geophys. Res. Lett.,* **38,** L12703, doi:10.1029/2011GL047436.

Mechoso, C. R., A. W. Robertson, C. F. Ropelewski, and A. M. Grimm, 2005: The American monsoon systems: An introduction. World Meteorological Organization Tech. Doc. WMO/TD 1266 (TMRP Rep. 70), 197–206.

Nieto-Ferreira, R., and T. M. Rickenbach, 2011: Regionality of monsoon onset in South America: A three-stage conceptual model. *Int. J. Climatol.,* **31,** 1309–1321.

Saha, S., and Coauthors, 2006: The NCEP Climate Forecast System. *J. Climate,* **19,** 3483–3517.

——, and Coauthors, 2010: The NCEP Climate Forecast System Reanalysis. *Bull. Amer. Meteor. Soc.,* **91,** 1015–1057.

Silva, A. E., and L. M. V. Carvalho, 2007: Large-scale index for South America Monsoon (LISAM). *Atmos. Sci. Lett.,* **8,** 51–57.

Silva, R. R., D. Werth, and R. Avissar, 2008: Regional impacts of future land-cover changes on the Amazon basin wet-season climate. *J. Climate,* **21,** 1153–1170.

Silva, V. B. S., V. E. Kousky, and R. W. Higgins, 2011: Daily precipitation statistics for South America: An intercomparison between NCEP reanalyses and observations. *J. Hydrometeor.,* **12,** 101–117.

Vera, C., G. Silvestri, B. Liebmann, and P. Gonzalez, 2006a: Climate change scenarios for seasonal precipitation in South America from IPCC-AR4 models. *Geophys. Res. Lett.,* **33,** L13707, doi:10.1029/2006GL025759.

——, and Coauthors, 2006b: Toward a unified view of the American monsoon systems. *J. Climate,* **19,** 4977–5000.

Wilks, D. S., 2006: *Statistical Methods in the Atmospheric Sciences.* 2nd ed. Academic Press, 648 pp.

Yuan, X., E. F. Wood, L. F. Luo, and M. Pan, 2011: A first look at Climate Forecast System version 2 (CFSv2) for hydrological seasonal prediction. *Geophys. Res. Lett.,* **38,** L13402, doi:10.1029/2011GL047792.

Zeng, N., J.-H. Yoon, J. A. Marengo, A. Subramaniam, C. A. Nobre, A. Mariotti, and J. D. Neelin, 2008: Causes and impacts of the 2005 Amazon drought. *Environ. Res. Lett.,* **3,** 014002, doi:10.1088/1748-9326/3/1/014002.